HOKKAIDO UNIVERSITY

Title	Steady state vapor compression refrigeration cycle simulation for a monovalent inverter-driven water-to-water heat pump with a desuperheater for low energy houses
Author(s)	Blanco, David L.; Nagano, Katsunori; Morimoto, Masahiro
Citation	International Journal of Refrigeration, 35(7), 1833-1847 https://doi.org/10.1016/j.ijrefrig.2012.07.005
Issue Date	2012-11
Doc URL	https://hdl.handle.net/2115/52252
Type	journal article
File Information	IJR35-7_1833-1847.pdf

Hokkaido University Collection of Scholarly and Academic Papers : HUSCAP

Steady state vapor compression refrigeration cycle simulation for a monovalent inverter-driven water-to-water heat pump with a desuperheater for low energy houses

David L. Blanco[1], Katsunori Nagano, Masahiro Morimoto

Division of Human Environmental Systems, Graduate School of Engineering. Hokkaido University, N13-W8. Kita Ku, Sapporo 060-8628, Japan

Abstract

A steady-state simulation is presented for a monovalent inverter-driven water-to-water heat pump with a desuperheater. For design-oriented simulations, superheating or subcooling degrees are used as input. However, the proposed simulation only uses the system's refrigerant charge, environmental, and control parameters, which make it particularly useful for off-design evaluations, including the annual performance factor calculation. Block models were used for the compressor and electronic expansion valve, while novel adaptive zone models were used for the heat exchangers. A multivariable error minimization algorithm was used over a sequential component scheme to provide global convergence. The numerical calculations were compared with 118 experimental results. The resulting COP agrees within 10% for 95.77% of the data. The mapping results reveal a maximum COP deviation of 8.78%. Computational results for the studied system reveal that a constant degree of superheating might not always maximize the COP.

Keywords:

Modeling; Simulation; Heat pump, Compression System; Hot water; Heating

[1] Corresponding Author
Email: david.blanco.ch@eng.hokudai.ac.jp , david.blanco.ch@gmail.com
Tel /Fax: +81-(0)11-706-6285

NOMENCLATURE

name	description	units	name	Description	units
		Roman characters			
A	Area	[m^2]	Pi	Pitch	[m]
$A_{0\ldots4}$	Constants	N.D.	Q	Heat transfer	[W]
$B_{0\ldots2}$	Constants	N.D.	R_{cu}	Thermal resistance	[WK^{-1}]
$C_{p/v}$	Specific heat at constant pressure or volume	[$Jkg^{-1}K^{-1}$]	*res*	Resolution	N.D.
ch	Number of channels	N.D.	*rug*	Rugosity	[m]
D	External diameter	[m]	*step*	Expansion valve step	N.D.
d	Internal diameter	[m]	*T*	Temperature	[K]
E	Error function	N.D.	*th*	Thickness	[m]
eval	Objective function	N.D.	*V*	Volume	[m^3]
f	Friction factor	N.D.	*v*	Specific volume	[m^3kg^{-1}]
freq	Electrical frequency of compressor	[Hz]	*vel*	Velocity	[ms^{-1}]
G	Volumetric flow rate	[m^3s^{-1}]	W_{com}	Compression work	[W]
H	Specific enthalpy	[Jkg^{-1}]	W_{el}	Compressor electric consumption	[W]
ht	Height	[m]	W_{is}	Isentropic work	[W]
L	Length	[m]	*wt*	Width	[m]
$\dot{m}$	Mass flow rate	[kgs^{-1}]	*x*	Quality	N.D.
M	Mass	[kg]			
M_{charge}	System's refrigerant mass charge	[kg]			
M_{tube}	Connection tubes' refrigerant mass content	[kg]			
N	Number of plates or turns	N.D.			
P	Pressure	[Pa]			
param	Parameters	N.D.			
		Greek characters			
α_{rug}	PHE rugosity factor	%	β	PHE chevron angle	*deg*
κ	Polytropic index	N.D.	η	Efficiency	N.D.
λ_{ev}	Specific enthalpy of Vaporization	[Jkg^{-1}]	ρ	Density	[kgm^{-3}]
μ	Viscosity	Pas	γ	Void fraction factor	N.D.
		Subscripts			
1,2,2',3,4	Junction number		*l*	Liquid zone	
c	Condenser		*m*	Mix zone	
compr	Compressor		*max*	Maximum	
cor	Corrugation		*min*	Minimum	
crit	Critical		*motor*	Compressor motor	
d	Desuperheater		*pass*	Number of passes	
e	Evaporator		*out*	Output of the zone	
eq	Equivalent		*r*	Refrigerant	
exp	Experiment		*sim*	Simulation	
expv	Expansion valve		*sw*	Swept	
fr	Friction		*trans*	Transversal	
g	Gas zone		*uc*	Uncompressible	
h	Hydraulic		*v*	Volumetric	
i	Component index (d, c, e)		*vac*	Vacuum	
in	Input of the zone		*z1,z2, z3*	First, second or third zone of heat exchanger	
is	Isentropic				
j	Zone index (l,g,m)				

1 Introduction

The new monovalent inverter-driven water-to-water heat pump with a desuperheater (compact GSHP with a desuperheater, Blanco et al., in press) can provide the thermal requirements for space heating (SH), cooling and domestic hot water (DHW) for a low energy house in a single unit with high efficiency and a stable output. Nevertheless, there has been only limited research regarding the operation and control of this system. Studies regarding a single frequency GSHP designed for SH that provides DHW by incorporating a desuperheater in its cycle are common in the literature (e.g., Biaou and Bernier, 2008). As no control techniques for frequency or expansion valves have been examined, the results of such studies can be misleading. A better understanding of the compact GSHP with a desuperheater requires a simulation program in which the design, control and evaluation of the system can be performed against changing climate conditions.

However, the refrigeration cycle simulations in the literature, as comprised in Table 1, lack two aspects needed for application to the compact GSHP with a desuperheater. First, they are design-oriented, such that the superheating/subcooling degrees or other performance characteristics are fixed (Hiller and Glicksman, 1976; Stefanuk et al., 1992; Hui and Spitler, 2002; Zhao et al., 2003; Rigola et al., 2005; Winkler et al., 2008; Belman et al., 2009). Therefore, while they can accurately reflect the behavior of the heat pump under ideal conditions, they fail to address the off-design conditions that can occur during the evaluation of the performance of a system throughout an entire year. Second, user-specified initial states of some or all of the thermodynamic variables of the cycle are required as a starting point to solve the algorithm (Hiller and Glicksman, 1976; Fukushima, et al., 1977; Domanski and Didion, 1984; Stefanuk et al., 1992; Koury et al., 2001; Hui and Spitler, 2002; Zhao et al., 2003; Rigola et al., 2005; Winkler et al., 2008; Belman et al., 2009). Because the state of the

refrigerant is not known, no unique set of initial conditions can be applied to all varying climate and load conditions. When the simulation runs for hundreds of cycles (e.g., to calculate the APF), manually checking the thermodynamic states for each condition becomes an impossible task. The process of identifying an initial condition needs to be transparent to the user.

The objective of this research is the development of a unique simulation for a compact GSHP with a desuperheater. In the presented simulation, a change in paradigm from a design-oriented simulation to a performance-oriented simulation is proposed. To address the first issue, the new simulation provides a flexible framework in which no performance parameters are assumed, relying instead on the characteristics of a real installation, namely, the refrigerant charge of the system and the existence of an unknown superheating degree. Additionally, fast adaptive block heat exchanger algorithms are developed to adjust to changing conditions. In this way, realistic subcritical cycles can be fully simulated, even under off-design conditions. Moreover, simulating different operation configurations is possible, such as SH only (mode 1), production of DHW only (mode 2) or for SH and DHW simultaneously (mode 3). The second issue is solved by identifying the solution space of each cycle variable based only on the climate and control inlet conditions to automatically determine a valid initial refrigerant state. Using this method, the simulation can be presented to the user as a black box which can be coupled with a ground heat transfer simulation and/or with a house heat transfer model to obtain a realistic performance estimate for the whole thermal system. This coupling allows the systematic calculation of the Annual Performance Factor (APF), which can be used to evaluate different control schemes.

2 Simulation development

Any vapor refrigeration cycle can be described in terms of components and junctions located in between (Richardson, 2006). Fig. 1 depicts the compact GSHP with a desuperheater. The junctions in the component view of Fig. 1(a) represent a unique refrigerant thermodynamic state. The state of these junctions is plotted on the PH diagram, shown in Fig. 1(b). Junction 2' can exist in either the mix or the gas zones, while junction 3 can exist in the gas, mix or liquid zone, depending on the inlet conditions. Because of the inherent trade-off in computing simulations between speed and detailed dynamic models, only the steady state is considered.

Finding the solution for a refrigeration cycle is subdivided into two subproblems:

- **Component modelling algorithms**: The output conditions for each component are determined according to its defined specific inlet conditions.
- **Cycle convergence algorithm**: The operating point of each of the junctions is determined to obtain a balanced solution among all of the components.

Two approaches have traditionally been used for the cycle convergence algorithm. Ding (2007) identifies the *simultaneous* and *sequential* solving methods. In this study, a carefully designed initial condition ensures that the sequential module method can be used to achieve convergence for all the study cases. As input, the simulation requires the geometrical information of the heat exchangers, the inlet temperatures and volumetric flow rates of the primary, secondary and DHW streams, and the control variables (expansion valve opening and compressor frequency). All the thermodynamic states of the junctions, the heat transferred at each heat exchanger, the electrical consumption of the compressor and the overall COP can be obtained as output. For each component, the main inlet and outlet variables are listed in Table 2.

This section will first introduce the assumptions and basic principles that were applied in the development of the simulation. Using these principles, three novel algorithms are introduced: The *generic adaptive zone heat exchanger model* uses boundary conditions to quickly solve the heat balance inside the heat exchangers for one, two or three refrigerant phases. This model is applied to the desuperheater, condenser and evaporator. The *mass flow rate conservation algorithm* defines the solution space of each junction in the system according to the inlet climate conditions and calculates the discharge pressure of the compressor based on the control conditions and an initial plausible state. Using the models developed, the *global convergence algorithm* maintains the heat and mass balance throughout each junction of the cycle. Finally, each component model is presented.

2.1. Assumptions

Four important assumptions are made in developing the simulation:

- *The model assumes perfect insulation of the system against its surroundings.*
- *It is assumed that there is no pressure drop in the condenser or desuperheater.*
- *It is assumed that complete evaporation occurs in the evaporator.*
- *It is assumed that the pressure change process inside the expansion valve is isenthalpic.*

2.2. Balance and conservation equations

As heat balance is maintained in every component, the overall system heat balance needs to be guaranteed. The heat extracted from the ground and the compression work should be equal to the heat delivered to the desuperheater and condenser:

$$Q_e + W_{com} - Q_d - Q_c = 0 \tag{1}$$

The pressure balance implies that the pressure increase in the compressor must be equal to the pressure decrease in the expansion valve and the pressure drop in the evaporator, as described by Eq. (2):

$$P_4 - P_1 - \Delta P_e = 0 \tag{2}$$

At the steady state, mass flow regulating devices should provide the same mass flow rate to obtain balance, as shown in Eq. (3):

$$\dot{m}_{expv} = \dot{m}_{compr} \tag{3}$$

The refrigerant mass content is a property of the system that remains constant at the steady state for any operating condition and any combination of inlet parameters. It has been suggested that when the mass charge is not considered, the simulation results are not from a unique system with different operating conditions, but are instead from many systems with different refrigeration charges (Stefanuk et al., 1992), which is incorrect for the purposes of this simulation. A mass balance implies that at every instant, the sum of the masses of all the components should be equal to the overall refrigerant charge, including the connection piping between components, which is described by Eq. (4):

$$M_{tube} = V_{tube}\rho_g\left(P_2\right) \tag{4}$$

The total mass in the system is then obtained using Eq. (5):

$$M_{compr} + M_d + M_c + M_e + M_{tube} = M_{charge} \tag{5}$$

2.3. Generic adaptive zone heat exchanger model

A novel generic algorithm for a counterflow heat exchanger, in which the geometry, the inlet temperatures and the stream flow rates are known, is presented. The model can successfully

adapt to different refrigerant zone combinations based on the changing inlet conditions. All of the possible zone combinations presented in Table 3 can be effectively modeled.

The algorithm is presented in Fig. 2. When a heat exchanger is examined, the overall heat transfer coefficients and the zone combinations of the heat exchanger are unknown because they depend on the particular inlet conditions. However, it is possible to monitor the available specific enthalpy change of each zone. To find the zone combination of a particular heat exchanger, a fast and easy solution is to assume initially that there is no phase change inside the heat exchanger, solve the system, and switch to a two or three zone case if the resultant enthalpy change is larger than the available enthalpy. For each zone, an average overall heat transfer coefficient is calculated and the NTU-ε method is applied. When the heat balance is obtained and the heat transfer area conservation is satisfied, the exchanger is solved, and the refrigerant mass content is calculated.

Solving the problem for one zone can be straightforward, but a change of phase requires solving the problem iteratively to guarantee balance. The developed method maintains the heat balance at every step, while iterating over a boundary variable to satisfy the heat transfer area conservation. The selection of the boundary variable will be addressed later in this section. To reduce the number of iterations, limits on the boundary variable are identified, and an error function based on these limits is constructed such that the initial problem is translated into a one dimensional bounded root searching problem. To solve it, Ridders' method (Ridders, 1979) is selected due to its low computing requirement and short calculation time.

2.3.1. Heat transfer area conservation and refrigerant mass content calculation

The available heat transfer area is the sum of the heat transfer area needed for each zone, as described in Eq. (6), where the sub index *i* is used to denote the appropriate heat exchanger:

$$A_{ig} + A_{im} + A_{il} = A_i \tag{6}$$

After finding a balanced solution for each heat exchanger, the refrigerant mass content must be calculated. The volume of refrigerant in each zone is proportional to the ratio of the heat transfer area for that zone to the total heat transfer area:

$$V_{ij} = \frac{A_{ij}}{A_i} V_i \tag{7}$$

where *j* represents the zone of consideration. The mass content of the gas or liquid zones is obtained directly from Eq. (8):

$$M_{ij} = V_{ij} \overline{\rho}_{ij} \tag{8}$$

To calculate the mass content in the mix zone, the analysis presented by Fukushima et al. (1969) is used, as follows:

$$M_{im} = V_{im} \gamma_{im} \rho_{ig} \left(1 - \gamma_{im}\right) \rho_{il} \tag{9}$$

where γ_{im} is the integral of the void fraction divided by the quality change, as described in Eq. (10):

$$\gamma_{im} = \frac{1}{x_{out} - x_{in}} \int_{x_{in}}^{x_{out}} \frac{x v_g}{x v_g + (1 - x) v_l} dx \tag{10}$$

The total mass content for the heat exchanger is the sum of the mass from each zone, as described in Eq. (11):

$$M_{ig} + M_{im} + M_{il} = M_i \tag{11}$$

2.3.2. Two zone boundary analysis

When a single phase change occurs inside the heat exchanger, the temperature of the secondary fluid when the refrigerant is in the saturated state, $T_{i,boundary}$, is used for iteration.

For a given $T_{i,boundary}$, an independent analysis is performed for each zone, starting in the same direction that the refrigerant flows. Initially, $A_{i\,z1}$ is determined using the NTU-ε method. The area of the second zone (A_{iz2}^{1}) is derived using heat transfer area conservation. Symmetrically, if the heat balance is calculated starting from the second zone, an additional value for the heat transfer area is determined (A_{iz2}^{2}). The difference between these two values is defined as an error function, as described in Eq. (12), below:

$$E_i\left(T_{i,boundary}\right) = A_{iz2}^{\ 1} - A_{iz2}^{\ 2} \tag{12}$$

2.3.3. Three zone boundary analysis

For the case with three zones, there exist two boundary temperatures for the secondary stream: one for the saturated vapor and one for the saturated liquid, at constant pressure P_2. However, these two temperatures are coupled through the heat transfer that occurs in the mix zone, so each can be expressed in terms of the other. As a result, the same methodology described above for two zones can be applied. Assuming condensation direction, $T_{i,boundary}$ is defined as the boundary temperature of the secondary fluid at the saturated liquid state. The boundary temperature for the saturated gas is then derived based on the enthalpy change that occurs in the mix zone. The gas and mix zone heat transfer areas can be calculated by the NTU-ε method. Through heat transfer area conservation, A_{iz3}^{1} is calculated. Applying the heat balance in the third zone produces A_{iz3}^{2}. The error function is then defined in the same way as the case with two zones.

$$E_i\left(T_{i,boundary}\right) = A_{iz3}^{\ 1} - A_{iz3}^{\ 2} \tag{13}$$

2.3.4. Mix zone analysis

In the condenser, when junctions 2' and 3 are located inside the mix zone, the average overall heat transfer coefficient changes depending on the condensation mode, which is related to the

enthalpy change. To find a balanced solution for this case, the exit enthalpy H_3 is selected as the boundary variable, in which case the same methodology described before can be applied. The error function can then be stated as

$$E_c(H_3) = A_m^{\ 1} - A_c \tag{14}$$

where $A_m^{\ 1}$ is derived from H_3 and A_c is the total heat transfer area of the heat exchanger, calculated based on geometric considerations.

2.4. Refrigerant mass flow rate conservation algorithm

The evaluation of the compressor and expansion valve components should provide an equal mass flow rate at the steady state. The difference between the two models can be defined as:

$$g(param, P_1, T_1, P_2) = \dot{m}_{compr} - \dot{m}_{expv} \tag{15}$$

which is a function of P_1, T_1 and P_2, assuming $P_4 = P_1 + \Delta P_e$. Thus, for a fixed point in junction 1, described by P_1 and T_1, the value P_2 can be obtained such that g is sufficiently small. To attain plausible junction 1 states, we rely on the application of the second law of thermodynamics to bracket the maximum and minimum values of the following variables:

- $T_1, T_4 \leq T_{e1}$: The temperature of the refrigerant at junction 1 or 4 cannot be greater than the inlet temperature from the primary side.
- $T_3 \geq \max(T_{c3}, T_{d2}')$: The temperature of the refrigerant at junction 3 cannot be less than the maximum temperature inlet from the secondary side.
- $P_2 \leq P_{crit}$: The cycle cannot be supercritical
- $P_1 > P_{vac}$: P_1 must be larger than the vacuum

The described conditions are plotted in the PH diagram shown in Fig. 3(a). The shaded regions represent the solution space for each junction. The limits for P_1, T_1 and P_2 can then be identified. Moreover, using $g = 0$ for a given T_1, the solution space for P_1 and P_2 can be

further narrowed as shown in the P_1-P_2 plane of Fig. 3(b). By setting limits that are based only on the inlet conditions, not only are the junction states carefully controlled inside the algorithm, but the algorithm also eliminates the need for the user to set an initial refrigerant thermodynamic condition.

From Fig. 3(a), it is observed that junction 1 is completely enclosed by the frontier temperature line T_{e1}, the vapor saturation line, and the pressure limits for P_1. Therefore, for a given P_1 and T_1 inside this region, finding P_2 is reduced to a single dimension root finding problem. Ridders' method is then applied.

2.5. Global convergence algorithm

The global convergence algorithm developed is composed of two core methods. The first method iterates through all the components of the cycle from an initial to a final state of junction 1, solving for each component. Successive substitution is used to resolve the pressure drop in the evaporator. The second method determines the error between the initial and final states of junction 1 and calculates the next iteration state to find convergence. In this case there are more than one boundary variables, so an analogy with the root finding method has to be developed. The multivariable global error function *eval* is defined in Eq. (16), in which T_1, T_1', H_1 and H_1' are respectively the initial and final temperatures and enthalpies of junction 1; and M_{charge} and M_{charge}' are the difference between the system's refrigerant charge and the calculated charge, respectively:

$$eval = \sqrt{\left(\frac{T_1 - T_1'}{T_{1\max} - T_{1\min}}\right)^2 + \left(\frac{H_1 - H_1'}{\lambda_{ev}}\right)^2 + \left(\frac{M_{charge} - M_{charge}'}{M_{charge,\max}}\right)^2} \qquad (16)$$

Convergence is translated into a multi-dimension minimization problem, in which the final solution is obtained for the enthalpy H_1 and the temperature T_1 that reduces the error function

below the desired resolution, while maintaining the appropriate balance. For the present simulation, the bounded Nelder-Mead method is selected according to Luersen et al. (2004) because other techniques require calculating the first-order derivate and the Hessian of *eval* at every step, which can be costly in terms of computing power. Additionally, at every step the solution is within the boundary limits, contrary to other techniques, in which iterations can reach prohibited spaces, such as in the Newton-Raphson method. To commence the algorithm, an initial simplex is constructed as the geometrical center point of the solution space of junction 1. The complete algorithm is described in Fig. 4.

2.6. Component modeling

2.6.1. Compressor

A model for the rotary type compressor with variable speed is developed. The inlet state of the refrigerant, the discharge pressure and geometrical parameters are taken as input. The model then calculates the mass flow rate $\dot{m}_{compr}$, the enthalpy of the discharged refrigerant H_2 and the compressor electric power W_{el}. The mass flow rate is determined from the compressor frequency and the swept volume as described in Eq. (17):

$$\dot{m}_{compr} = \eta_v \rho_1 V_{sw} freq \tag{17}$$

where η_v is the volumetric efficiency described by Eq. (18):

$$\eta_v = 1 + \frac{V_{uc}}{V_{sw}} - \frac{V_{uc}}{V_{sw}} \left(\frac{P_2}{P_1} \right)^{\kappa} \tag{18}$$

Here, the adiabatic index is calculated from junction 1. The electrical power consumption is described by Eq. (19):

$$W_{el} = \frac{W_{com}}{\eta_{motor}} \tag{19}$$

where the motor loss efficiency η_{motor} is evaluated according to Chen et al. (2002) from Eq. (20):

$$\eta_{motor} = A_0 + A_1\, freq + A_2 W_{is} + A_3 \ln\left(\frac{P_2}{P_1}\right) + A_4 W_{is} \ln\left(\frac{P_2}{P_1}\right) \tag{20}$$

where W_{is} is the isentropic work, calculated using Eq. (21):

$$W_{is} = \dot{m}_{compr} \frac{\kappa}{\kappa - 1} \frac{P_1}{\rho_1} \left[\left(\frac{P_2}{P_1}\right)^{\frac{\kappa-1}{\kappa}} - 1 \right] \tag{21}$$

The actual compression process is related to the ideal process by the friction efficiency. For the present study, the friction efficiency is considered constant. Eq. (22) is then used to derive the compression work:

$$W_{com} = \frac{W_{is}}{\eta_{fr}} \tag{22}$$

The discharge enthalpy of the refrigerant can then be determined from the compression work, as described by Eq. (23):

$$H_2 = H_1 + \frac{W_{com}}{\dot{m}} \tag{23}$$

The refrigerant mass content in the compressor is calculated from the swept volume at the average density of the refrigerant through the compression process, as shown in Eq. (24):

$$M_{compr} = V_{sw} \overline{\rho}_{12} \tag{24}$$

where $\overline{\rho}_{12}$ refers to the arithmetic mean density between junctions 2 and 1.

2.6.2. Desuperheater

The desuperheater model is based on a horizontal, double-tube, coil-type heat exchanger, as shown in Fig. 5(a). While the refrigerant inlet (junction 2) is always in the gas zone, the zone for the exit of the refrigerant (junction 2') varies. Applying the generic heat exchanger model

yields two cases, as follows: (*case DGG)* when the exit of the heat exchanger is still in the gas phase and *(case DGM)* when the exit has started condensing. The overall heat transfer coefficient is calculated for each zone based on the specific geometrical characteristics and heat transfer correlations, and it is included in Appendix A.

For the DGG case, the solution is obtained directly by applying the NTU-ε method. The DGM case is solved by applying the generic heat exchanger model for two zones. The conservation of the heat transfer area is maintained by setting A_{dl} = 0 in Eq. (6). To apply Ridders' method, the boundary temperature T_{d6} is selected for iteration. The T_{d6} limits are calculated using Eqs. (25) and (26). The error function is defined, as stated in Eq. (12), for *i* = *d* and *z2* = *m*.

$$T_{d6}^{\max} = \min\left(T_2 - \frac{Q_{dg}}{\min\left(C_{pw}\dot{m}_w, C_{pg}\dot{m}\right)}, T_6 \right) \tag{25}$$

$$T_{d6}^{\min} = T_{d2}' \tag{26}$$

2.6.3. Condenser

The condenser and evaporator are modeled as brazed plate type, single pass, and water to water heat exchangers, as shown in Fig. 5(b). Depending on the heat transfer in the desuperheater, junction 2' can be either in the gas or mix zone. Similarly, junction 3 can be in the gas, mix or liquid zone, depending on the heat transfer in the condenser. The combination of these inlet-outlet relationships results in five cases: CGG, CGM, CGL, CMM, and CML.

The CGG case is solved by direct application of the NTU-ε method. The generic heat exchanger model is applied to solve the CGM case, where T_{c6} represents the boundary

temperature. The limits are found using Eqs. (27) and (28). The error function is obtained by setting $i = c$ and $z2 = m$ in Eq. (12).

$$T_{c6}^{\max} = \min\left(T_2' - \frac{Q_{cg}}{\min\left(C_{pc}\dot{m}_c, C_{pg}\dot{m}\right)}, T_6\right) \tag{27}$$

$$T_{c6}^{\min} = T_{c3} \tag{28}$$

To apply the generic heat exchanger algorithm to the three zone case for CGL, the limits of the boundary temperature T_{c7} are determined using Eqs. (29) and (30). From Eq. (13), the error function is determined with $i = c$ and $z3 = l$.

$$T_{c7}^{\max} = \min\left(T_2' - \frac{Q_{cg}}{\min\left(C_{pc}\dot{m}, C_{pg}\dot{m}\right)} - \frac{Q_{cm}}{C_{pc}\dot{m}},\ T_6 - \frac{Q_{cm}}{C_{pc}\dot{m}}, T_{c3} + \frac{Q_{cl}^{\max}}{C_{pc}\dot{m}}, T_7\right) \tag{29}$$

$$T_{c7}^{\min} = T_{c3} \tag{30}$$

The CMM case is solved based on the mix zone analysis from subsection 2.3.4. The limits on H_3 are shown in Eqs. (31) and (32). The error function is described by Eq. (14).

$$H_3^{\max} = H_2' \tag{31}$$

$$H_3^{\min} = H_7 \tag{32}$$

The CML case is solved in the same way as the CGM case. The limits of the boundary temperature T_{c7} are obtained from Eqs. (33) and (34). The error is determined using Eq. (12), where $i = c$ and $z2 = l$.

$$T_{c7}^{\max} = \min\left(T_{2'} - \frac{Q_{cm}}{C_{pc}\dot{m}}, T_{c3} + \frac{Q_{cl}^{\max}}{C_{pc}\dot{m}}, T_7\right) \tag{33}$$

$$T_{c7}^{\min} = T_{c3} \tag{34}$$

2.6.4. Expansion valve

The electronic expansion valve is modeled based on the pressure drop across an orifice. The Chuan et al. (2006) modified model is used. Eq. (35) shows the resulting mass flow rate with controlled steps:

$$\dot{m}_{expv} = \eta_{expv}\rho_{3l}\left[B_0\left(\frac{step}{A_{\max}}\right)^2 + B_1\left(\frac{step}{A_{\max}}\right)\right]\sqrt{B_2\left(\frac{P_2 - P_4}{\rho_{3l}}\right)} \tag{35}$$

where $A_{\max}$ represents the maximum opening of the expansion valve. Because the expansion valve is modeled as an orifice, it is assumed that the valve contains no refrigerant mass.

2.6.5. Evaporator

The enthalpy of junction 4 is the same as junction 3 but at pressure P_4 and is in the mix zone. The exit of the evaporator (junction 1) is assumed to be in the gas zone, resulting in case EMG. To solve this case, the limits of the boundary temperature T_{e5} are obtained from Eqs. (36) and (37). Eq. (12) is used to determine the error where $i = e$ and $z2 = g$.

$$T_{e5}^{\max} = T_{e1} \tag{36}$$

$$T_{e5}^{\min} = \max\left(T_{e1} - \frac{Q_{eg}^{\max}}{C_{pe}\dot{m}}, T_4 + \frac{Q_{em}}{C_{pe}\dot{m}}, T_5\right) \tag{37}$$

The experimental results reveal that while the condensing pressure drop can be on the order of 10^1 Pa, the evaporator pressure drop can be on the order of 10^3 Pa, therefore it is considered. The pressure drop is calculated based on the work by Han et al. (2003).

3 Experimental Setup

Simulation results were compared with experiments conducted on a prototype compact GSHP with a coil type desuperheater developed by Sunpot Co. Ltd. The compact GSHP uses refrigerant R410A with a nominal charge of 1.8 kg. The prototype was coupled with a test

station developed by the authors, which can be used to examine the performance of any water-to-water heat pump. All the components and connection pipes were tightly covered with EPT/EPDM insulation with an R-value of 4.1. Analysis on the pipes revealed a maximum heat loss for water of 18.21 Wm^{-1}. Ambient temperature was maintained between 20 and 24°C throughout the experiments. The examined conditions are shown in Table 4. Detailed information is found in (Blanco et al., in press). 118 experimental results of the system operating in mode 3 were extracted for this study.

4 Results and discussion

4.1. System simulation results

To examine the precision of the developed simulation, it was executed for the same inlet conditions as the experimental data. The heat transfer of each heat exchanger, W_{el} and the COP calculated as the ratio of the total heating output to the compressor's electrical input, were compared. The results are shown in Fig. 6. W_{el} has a maximum deviation with the experimental results of less than 10%. For Q_d, only 6.78% of the data has a total deviation greater than 15%. For Q_c and Q_e, the deviations are 7.62% and 12.7%, respectively. Examining the COP, only 4.23% of the results show a difference greater than 15% compared to the experimental data. Consequently, the simulation exhibits good agreement with the experimental results. However, the previous analysis is not sufficient to show the versatility of the simulation. The equation fitted models show equivalent results to the experimental work. However, they cannot describe the thermodynamic states of each junction in the cycle. The developed simulation has this capability, as shown in the next subsection.

4.2. Simulated refrigeration cycles

Fig. 7 shows two PH diagram comparisons between experimental and simulated results for various inlet conditions. It can be seen that the simulation successfully fits the changing climate and control conditions. The numerical comparison of the junctions is presented in Table 5, and the highest relative error, calculated using Eq. (38), is less than 3% for all the junctions:

$$\text{relative error}\,\% = \sqrt{\left(\frac{H_{\text{exp}} - H_{\text{sim}}}{H_{\text{exp}}}\right)^2 + \left(\frac{P_{\text{exp}} - P_{\text{sim}}}{P_{\text{exp}}}\right)^2} \tag{38}$$

It has been shown that the model can predict well the refrigeration cycles in the PH diagram. However, to provide further clarity, a systematic performance analysis regarding changing climate conditions is presented.

4.3. Mapping results

The maximum COP and total heat transfer for the set of evaluated climate and control conditions are compared with the experimental results in the maps shown in Fig. 8 with T_{d2}' = 5 and 17°C. This figure is extremely important not only for showing the maximum COP that can be achieved for each frequency at a given ground inlet temperature based on the target T_{c2}' and T_{d2}, but it also indicates the wide range of climate conditions the simulation can correctly predict. In fact, the maximum deviation with experimental results was 8.78% for the COP and 11.61% for the total heat transfer.

4.4. Application of the simulation to various operation modes

After demonstrating the robustness of the simulation against changing conditions and strong precision with respect to experimental results, a unique feature is presented. So far, only one operation mode has been investigated, in which DHW is produced together with SH. Nevertheless, the real operation of the system requires the ability to handle other operation

modes. Fig. 9 shows the operation of the system for modes 1, 2 and 3. While the cycles of mode 1 and 3 do not substantially change, the condensation pressure in mode 2 is much higher than in the other two modes. This characteristic behavior of the GSHP with a desuperheater can be exploited using this unique simulation for control analysis, according to the set operation mode.

4.5. Superheating degree control

Fig. 10 shows the variation of the COP according to the change in the opening of the expansion valve. For mode 1 in Fig. 10(a), the highest COP occurred with a superheating degree of 8.1°C, while for mode 3 in Fig. 10(b), the highest COP occurred with a superheating degree of 9.8°C. In mode 3 it is important to note that for higher expansion valve steps, the refrigerant temperature at the compressor outlet is lower than the DHW objective temperature, therefore cannot be considered. For the same system and refrigerant charge, the highest COP occurs at different values, suggesting that setting a fixed superheating degree may not necessarily be the best strategy for maximizing the COP.

5 Conclusions

An original vapor refrigerant cycle simulation was constructed for a compact GSHP with a desuperheater based only on the refrigerant charge, the physical parameters of the components and the control parameters. An analysis of the boundary conditions was performed to define the solution space in which the states of the junctions of the system are located. Using a sequential component solving algorithm and adaptive zone models for the heat exchangers, global convergence was achieved using multidimensional error minimization techniques. The simulation is capable of predicting space heating or cooling capacities, domestic hot water generation heat transfer and compressor power. Furthermore,

the simulation successfully models different operation modes of the system, such as space heating only, domestic hot water only, and a combination of the two.

A prototype GSHP with a desuperheater was constructed, and experiments were conducted. Comparing the experimental data, which covered extensive climate conditions, the simulation results showed that for the COP, only 4.23% of the results have a deviation greater than 15% (showing the range of application and the precision of the simulation).

Using the simulation, it was shown that the highest COP for space heating only mode and combined space heating and domestic hot water production, occur at different superheating degrees, suggesting that a constant superheating degree strategy may not provide the highest COP for all operating conditions.

Finally, a complete mapping of the maximum COP and the total heat transfer occurring under the tested climate conditions was performed to compare the simulated and experimental results. This comparison showed a maximum deviation of 8.78% for the COP and 11.61% for the total heat transfer. The results indicate that the simulation can be used to test different control techniques and parameter variations to increase the overall system COP and to simulate off-design conditions.

Acknowledgements

The authors would like to thank Mr. Niki, Mr. Okamoto and Mr. Uchino from Sunpot Co. Ltd. for their insight into the prototype machine. In addition, we would like to thank Mr. Nakamura from Hokkaido University for his help with the development of the experiments, and we thank Ph.D. Katsura and Mr. Umezawa, formerly from Hokkaido University, for their

fruitful discussions. The financial support from the Ministry of Education, Culture, Sports, Science and Technology of Japan is also greatly appreciated.

Appendix A. Area calculation and heat transfer correlations for heat exchanger heat transfer

A.1 Desuperheater

The overall heat transfer coefficient is determined based on the geometrical parameters and the mass flow rates of the refrigerant and water streams. The total heat transfer area is calculated using Eq. (A.1-1):

$$A_d = N_d \sqrt{\pi D_d^{\,2} + Pi^2}\left(wt_d + c\right) \qquad 1)$$

where $c = 3^{-1}\pi d_d$ represents the contact surface between the hot and cold tubes of the desuperheater. The equivalent diameter for the tubes is calculated using Eq. (A.1-2):

$$d_h = \frac{4}{2\cdot wt_d + \pi\cdot d_d}\left[d_d \cdot wt_d + \left(\frac{\pi\cdot d_d^{\,2}}{4}\right)\right] \qquad 2)$$

The transversal area is calculated using Eq. (A.1-3), and the total volume is determined using Eq. (A.1-4). To derive the overall convective heat transfer, it is necessary to determine the average bulk velocity for each of the fluids, as described in Eq. (A.1-5):

$$A_{d\,trans} = \frac{\pi\cdot d_d^{\,2}}{4} + wt_d \cdot d_d \qquad 3)$$

$$V_d = A_{d\,trans} N_d \sqrt{\pi D_d^{\,2} + Pi^2} \qquad 4)$$

$$vel_d = \frac{\dot{m}}{\rho_d A_{d\,trans}} \qquad 5)$$

Using these velocities and the refrigerant and water properties, the Reynolds and Prandtl numbers can be derived. Using the hydraulic diameter, the friction factor for the tubes can be calculated according to Haaland (1983). The Nusselt number for a single phase in straight

tubes is calculated according to Gnielinski (1976). This correlation is used for single phase streams. Additionally, the coil heat transfer enhancement proposed by Schmidt (1967) is used. The convective heat transfer coefficient can then be derived for each stream.

In the mix zone, the correlation provided by Shah (1981) is applied. For the liquid state, Gnielinksi's correlation with curvature for the refrigerant at the same pressure in the saturated liquid state is used. From the respective convective heat transfer coefficient for both streams, the overall heat transfer coefficient can be derived for each zone.

A.2 Condenser and evaporator

Because the condenser and evaporator heat exchangers are identical, the heat transfer area for each can be determined using Eq. (A.2-1):

$$A_i = (N_i - 2) ht_i wt_i \alpha_{rug} \quad 1)$$

The transversal channel area is described by Eq. (A.2-2), and the total volume of the heat exchanger is described by Eq. (A.2-3):

$$A_{itrans} = wt_i \left(\frac{L_i - N_i th_i}{N_i - 2} \right) \quad 2)$$

$$V_i = wt_i \left(\frac{L_i - N_i th_i}{2} \right) ht_i \quad 3)$$

The equivalent hydraulic diameter is determined using Eq. (A.2-4):

$$d_{ih} = \frac{2A_{itrans}}{wt_i + \frac{A_{itrans}}{wt_i}} \quad 4)$$

Gnielinski's correlation is used for both streams when there is no change of phase. For the condensation zone, the correlation provided by Shah is applied. For evaporation, the method proposed by Kandlikar (1990) is applied. The overall heat transfer coefficient can therefore be calculated for each zone.

References

Belman, J. M., Navarro-Esbrí, J., Ginestar, D., Milian, V., 2009. Steady-state model of a variable speed vapor compression system using R134A as working fluid. Int. J. Energy Res. 34(11), 933-945.

Biaou, A. L., Bernier, M. A., 2008. Achieving total domestic hot water production with renewable energy. Build. Environ. 43, 651-660.

Blanco, D.L., Nagano, K., Morimoto, M., in press. Experimental study on a monovalent inverter-driven water-to-water heat pump with a desuperheater for low energy houses, Appl. Therm. Eng., doi: 10.1016/j.applthermaleng.2012.07.008.

Chen, Y., Halm, N. P., Braun, J. E., Groll, E. A., 2002. Mathematical modeling of scrolls compressors-part II: Overall scroll compressor modeling. Int. J. Refrigeration 25, 751-764.

Chuan, Z., Shanwei, M., Jiangpin, C., Zhijiu, C., 2006. Experimental analysis of R22 and R407C flow through electronic expansion valves. Energy Convers. Manage. 47, 529-544.

Ding, G., 2007. Recent developments in simulation techniques for vapour-compression refrigeration systems. Int. J. Refrigeration 30, 1119-1133.

Domanski, P., Didion, D. 1984, Mathematical model of an air-to-air heat pump equipped with a capillary tube. Int. J. Refrigeration **7**(4), 249-255.

Fukushima, T., Arai, A., Arai, N., 1977. Simulation of refrigeration cycle for air conditioners. JSRAE Reito 52 (593), 301-314.

Gnielinski, V., 1976. New equations for heat and mass transfer in turbulent pipe and channel flow. Int. Chem. Eng., 16, 359-368.

Haaland, S. E., 1983. Simple and explicit formulas for the friction factor in turbulent pipe flow. J. Fluids Eng. 105, 89-90.

Han, D.H., Lee, K.J., Kim, Y.H., 2003. Experiments on the characteristics of evaporation of R410A in brazed plate heat exchangers with different geometric configurations. Appl. Therm. Eng. 23, 1209-1225.

Hiller, C. C., Glicksman, L. R., 1976. Improving heat pump performance via compressor capacity control - analysis and test. Technical report, Massachusetts Institute of Technology.

Hui Jin, Spitler, J.D., 2002. A parameter estimation based model of water-to-water heat pumps for use in energy calculation programs. ASHRAE Transactions 108 (1), 3-17

Kandlikar, S., 1990. A general correlation for saturated two-phase flow boiling heat transfer inside horizontal and vertical tubes. J. Heat Transfer 112, 219-228.

Koury, R.N.N., Machado, L., Ismail, K.A.R., 2001. Numerical simulation of a variable speed refrigeration system. . Int. J. Refrigeration **2**4, 192-200.

Luersen, M., Le Riche, R., Guyon, F. 2004, A constrained, globalized, and bounded Nelder Mead method for engineering optimization, Struct. Multidiscip. O. 27, 43-54.

Richardson, D., 2006. An object oriented simulation framework for steady-state analysis of vapor compression refrigeration systems and components. Ph.D. thesis dissertation, University of Maryland.

Ridders, C., 1979. A new algorithm for computing a single root of a real continuous function. Trans. Circuits Syst. Vol. CAS-26 (11), 979-980.

Rigola, J., Raush, G., Pérez-Segarra, C.D., Oliva, A., 2005. Numerical simulation and experimental validation of vapor compression refrigeration systems. Special emphasis on CO_2 trans-critical cycles. Int. J. Refrigeration 28, 1225-1237

Schmidt, E. 1967, Wärmeübergang und druckverlust in rohrschlangen, Chem. Ing. Tech. 39(13), 781-789.

Shah, M. M. 1981, Heat transfer during film condensation in tubes and annuli; a literature survey. ASHRAE Transactions 87 (1), 1086-1105.

Stefanuk, N. M., Aplevich, J. D., Renksizbulut, M., 1992. Modeling and simulation of a Superheat-controlled water-to-water heat pump. ASHRAE Transactions 98(2), 172-184.

Winkler, J1., Aute, V., Radermacher, R., 2008. Comprehensive investigation of numerical methods in simulating a steady-state vapor compression system. Int. J. Refrigeration 31, 930-

942.

Zhao, P.C., Ding, G.L., Zhang, L., Zhao, L., 2003. Simulation of a geothermal heat pump with non-azeotropic mixture, Appl. Therm. Eng. 23, 1515-1524.

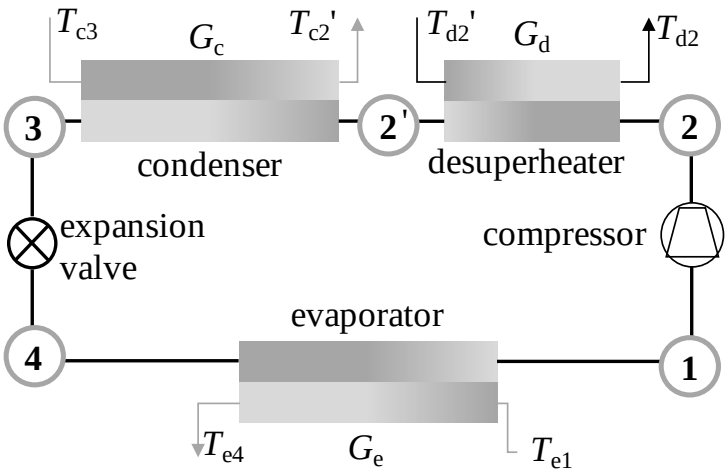

a) Component diagram

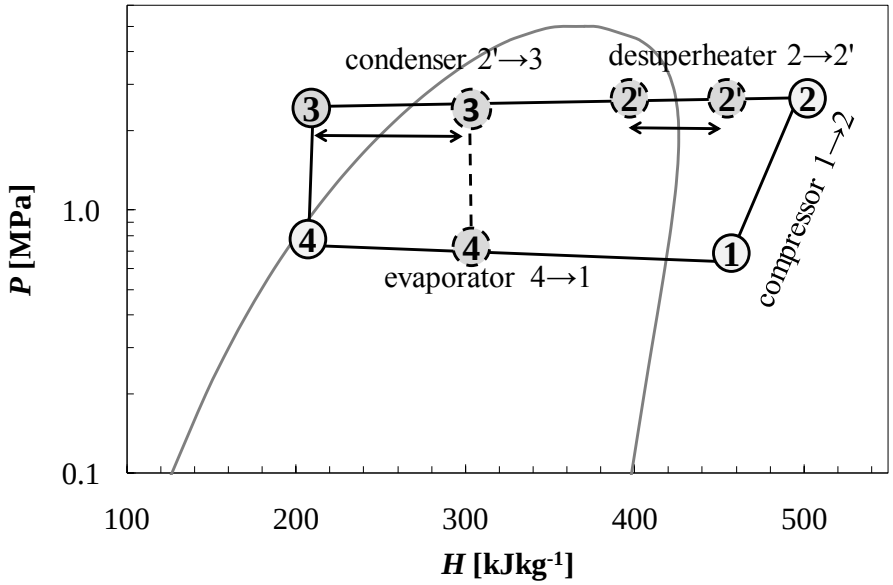

b) Representation in the PH diagram

Fig. 1. Compact GSHP with desuperheater

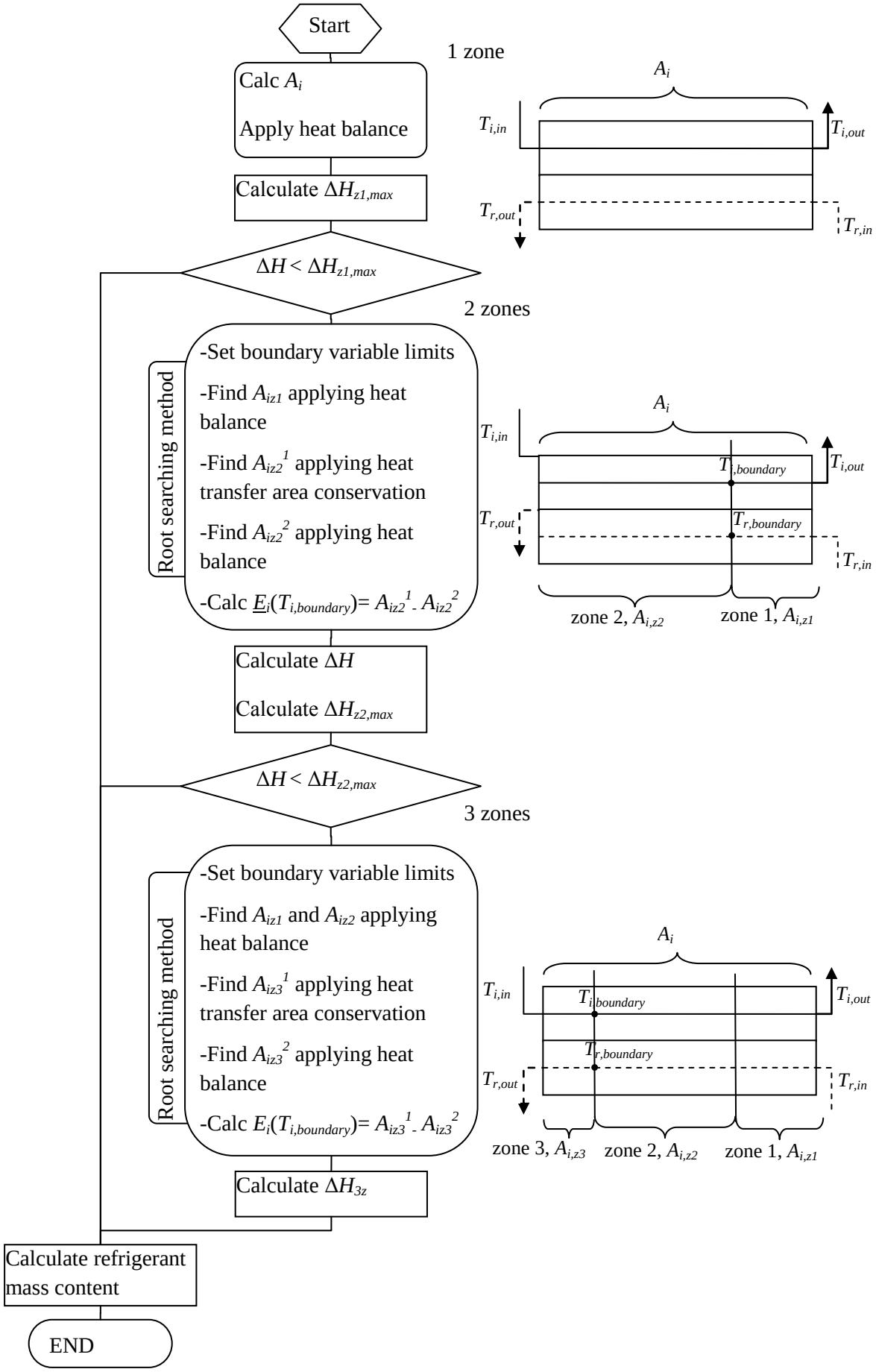

Fig. 2. Generic adaptive zone heat exchanger model

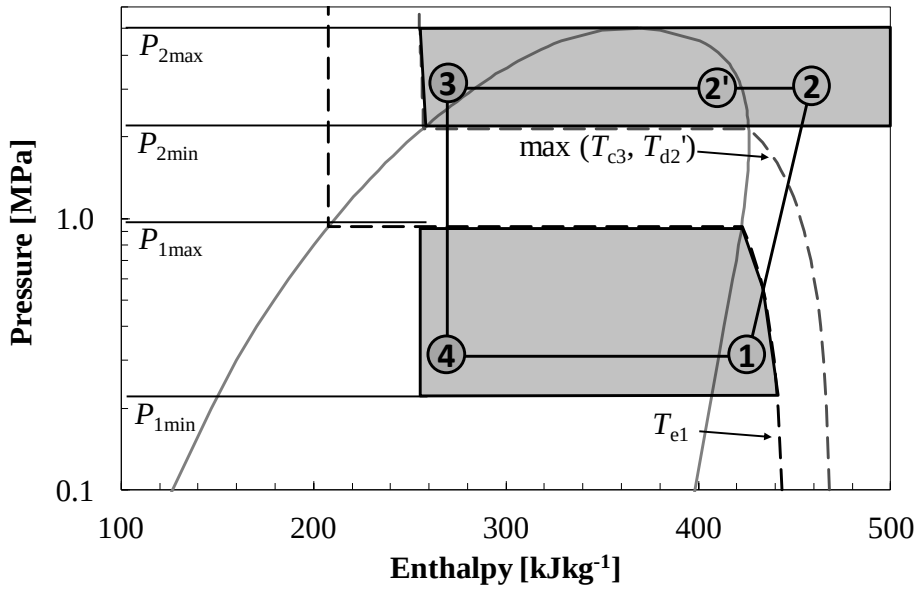

a) Solution space for the cycle junctions based on inlet conditions

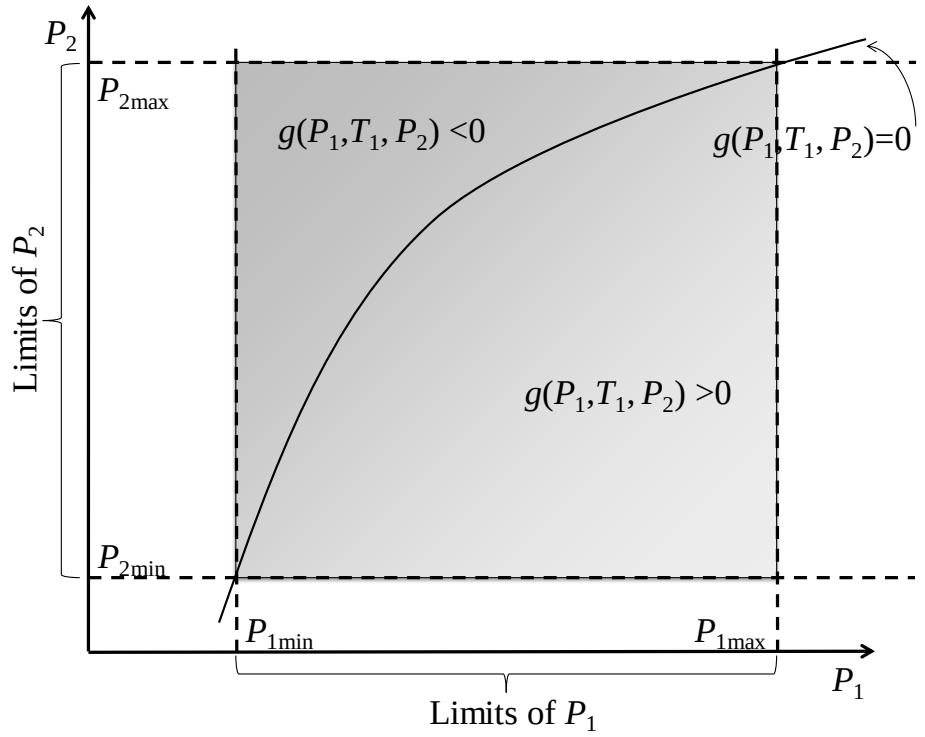

b) The limits for the suction pressure P_1 are set according to the limits of the discharge pressure P_2. The function g expresses the difference between the mass flow rate calculated by each regulation device in the cycle. The solution for P_1, T_1, and P_2 represents a point that must exist on the line g within the shaded region

Fig. 3. Solution space for each junction based on the refrigerant mass flow rate conservation algorithm

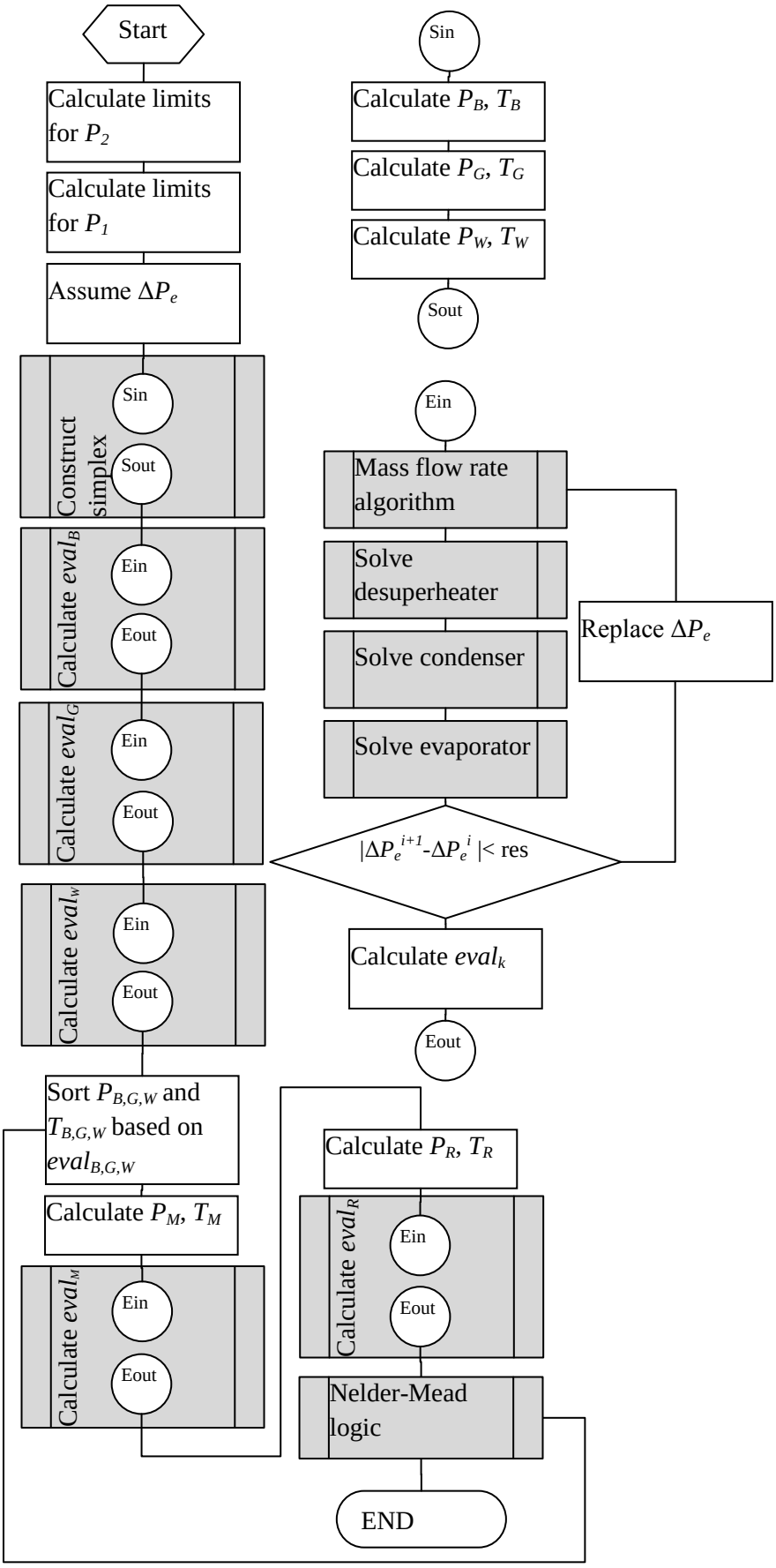

Fig. 4. Global convergence algorithm

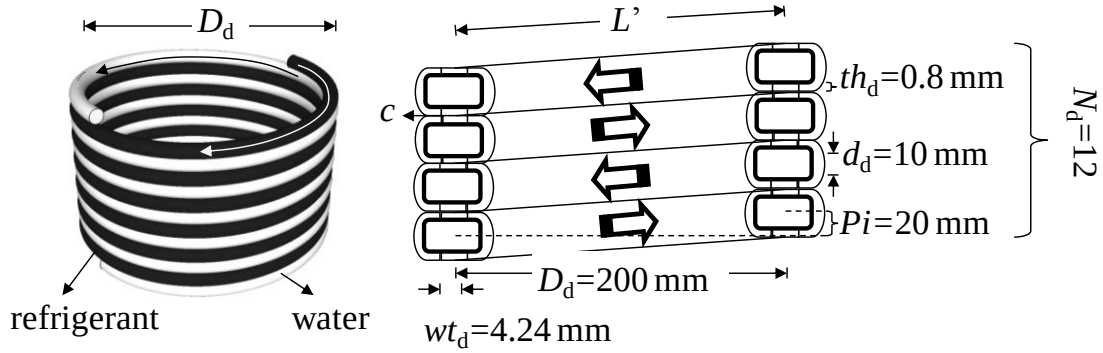

a). Indirect contact coil type desuperheater

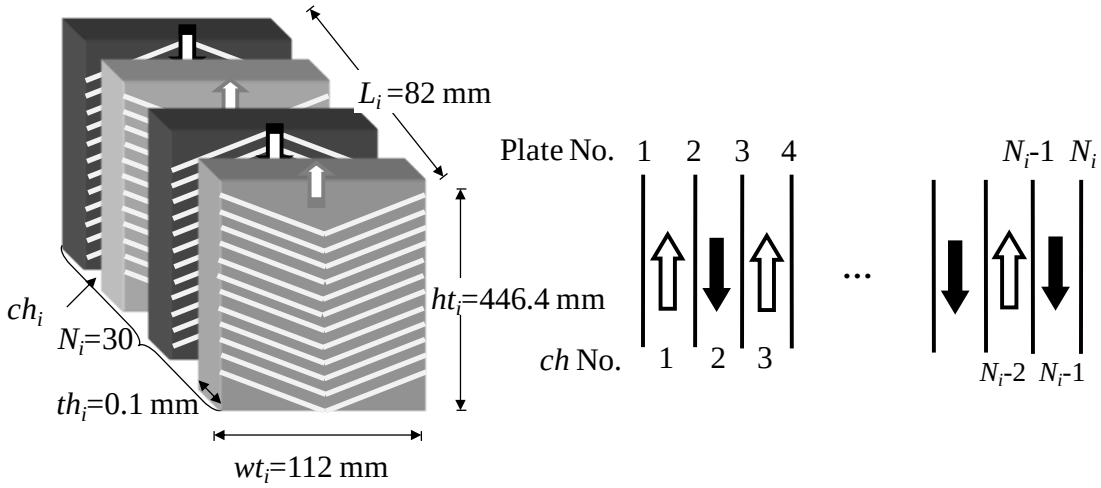

b) Condenser and evaporator plate type heat exchangers

Fig. 5. Geometrical parameters of the heat exchanger components of the prototype

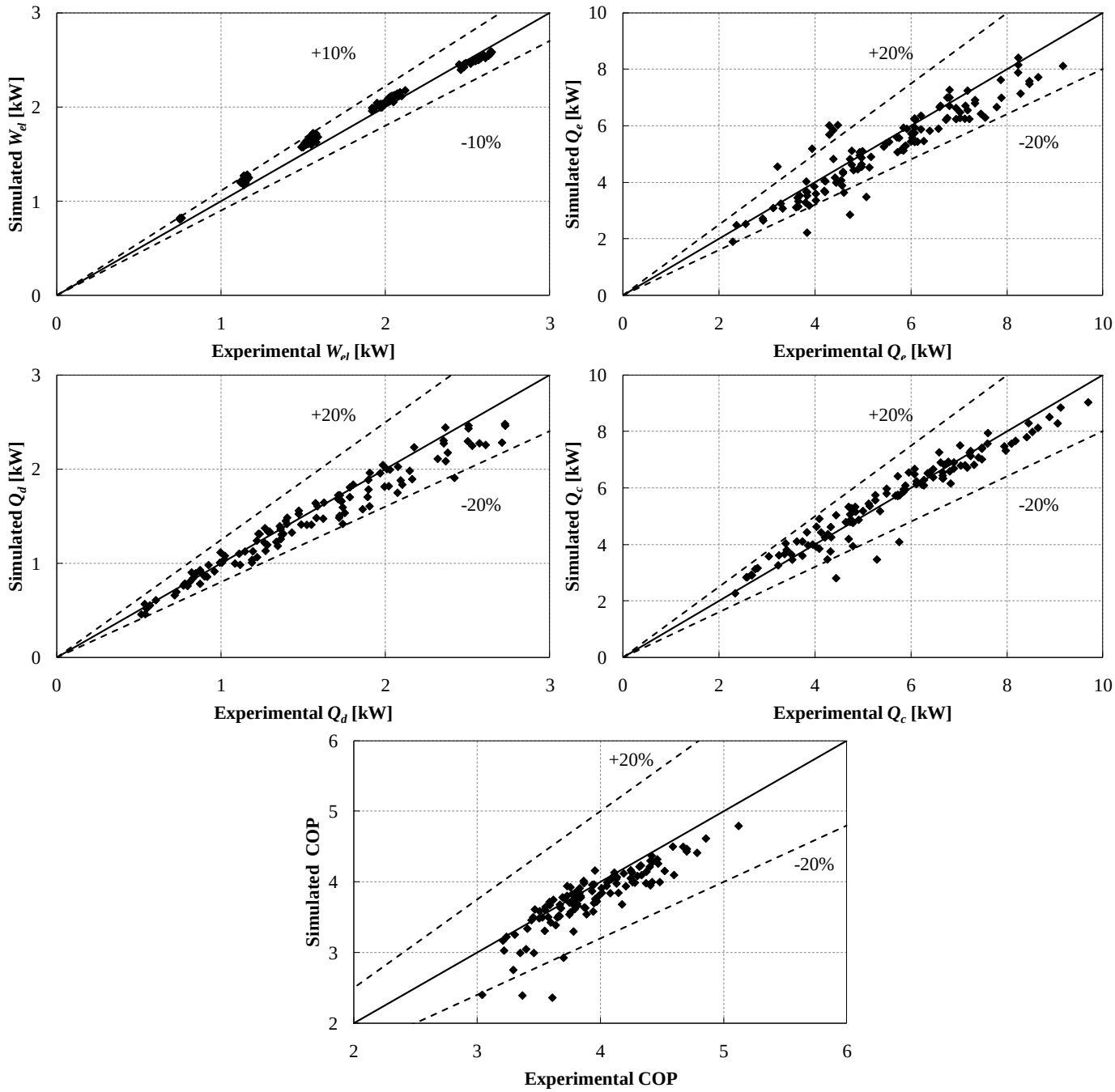

Fig. 6. Complete system comparison between experimental and simulation results

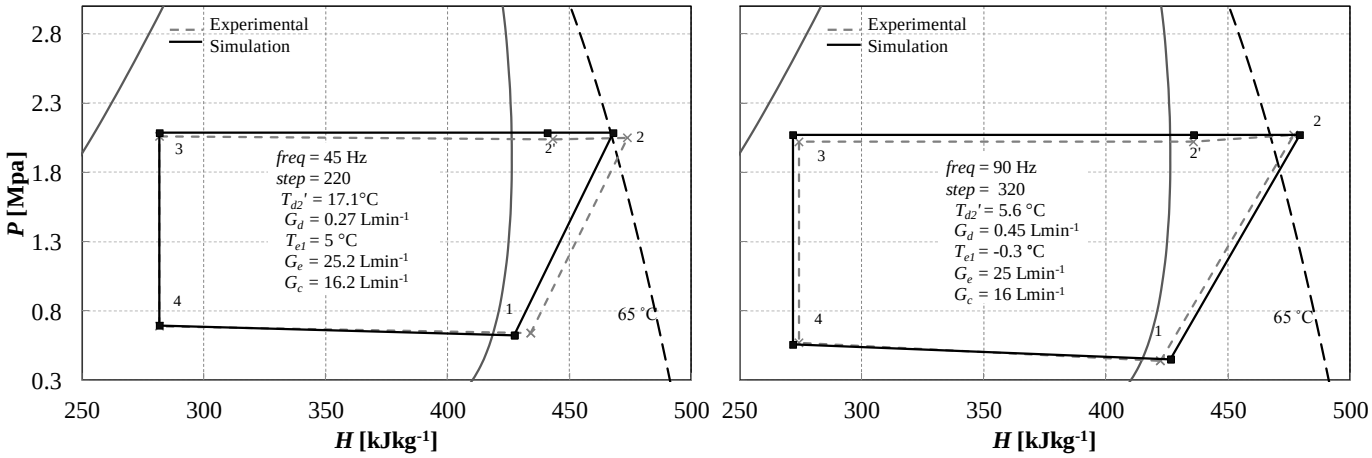

Fig. 7. Comparison between simulated and experimental refrigeration cycles in the PH diagram.

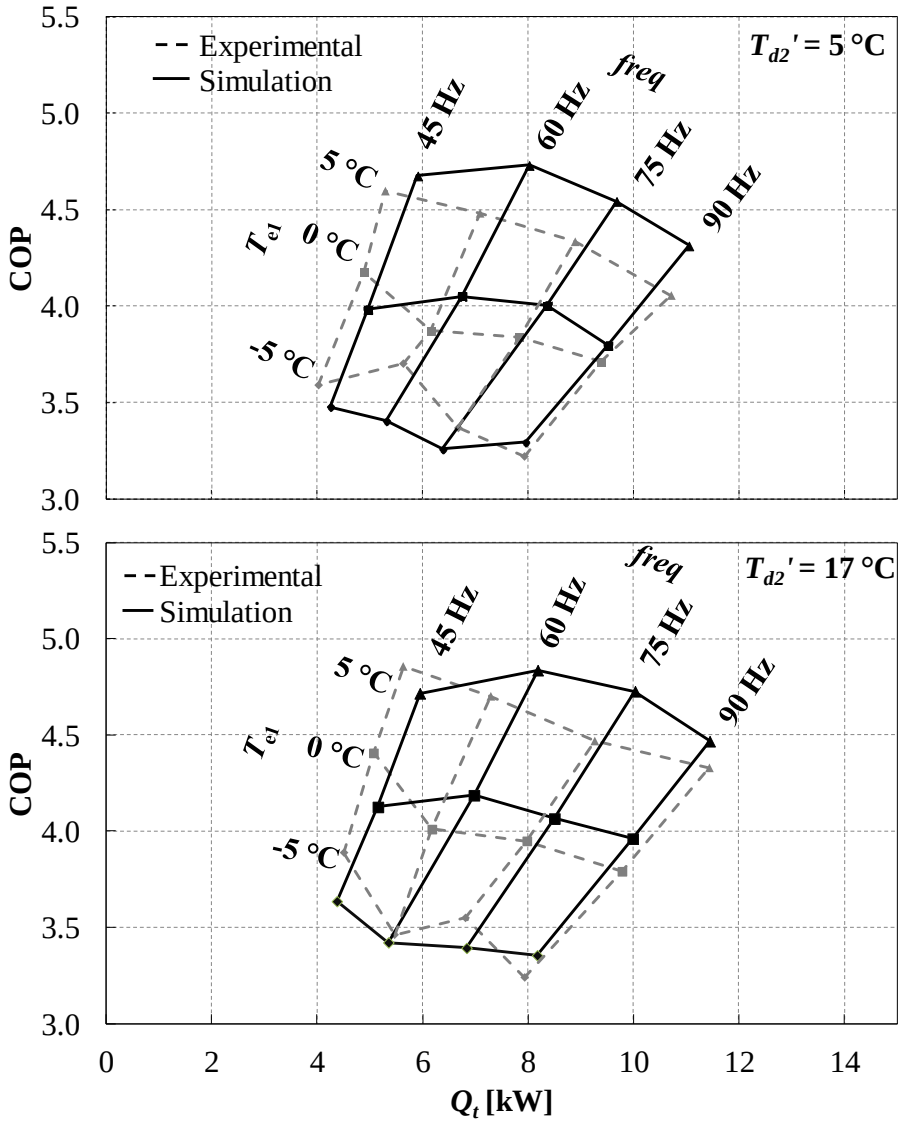

Fig. 8. Comparison of mapping results for T_{d2}' = 5°C and 17°C between experimental and simulation results

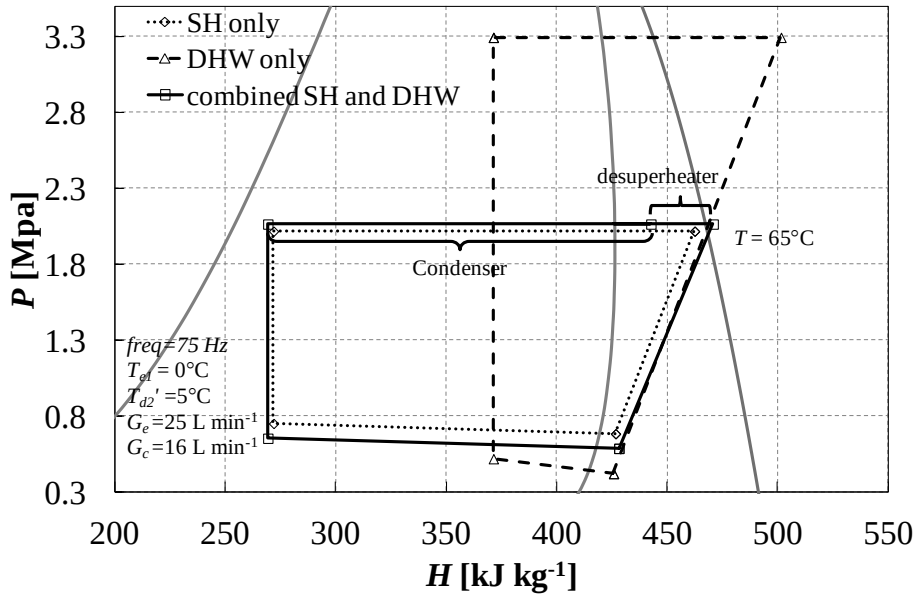

Fig. 9. Simulation results for the compact GSHP with a desuperheater for three of its operation modes under the same climate conditions

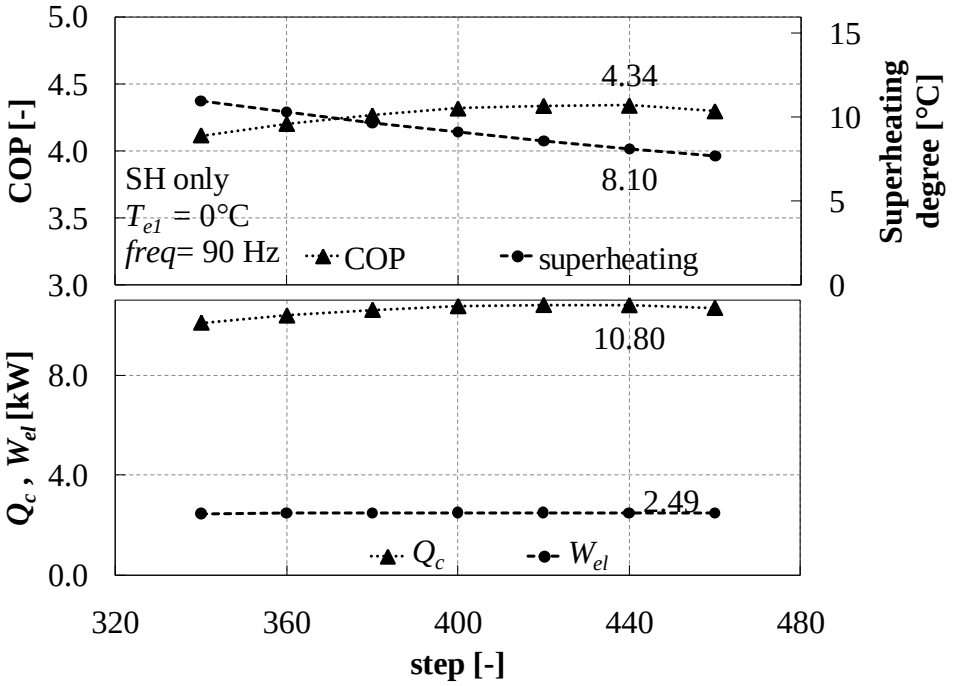

a) Space heating only

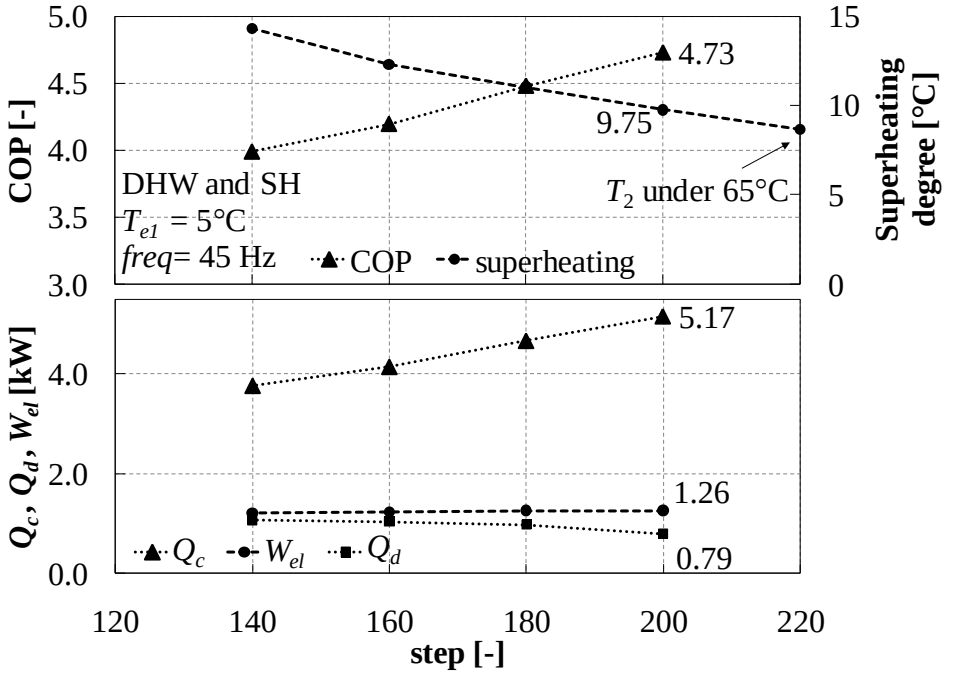

b) Combined space heating and domestic hot water

Fig. 10. Simulated superheating with expansion valve control

Table 1. Selected vapor compression refrigeration cycle simulations

Authors, year	Considerations	System analysis	Compressor speed	Heat exchangers models	Expansion device	Convergence technique	Simulation application
Hiller and Glicksman (1976)	-Fixed superheating and subcooling degrees -Fixed evaporating temperature	Steady	Variable	-No desuperheater - Three and two zones for the condenser and evaporator, respectively	- Thermostatic expansion valve	-Dichotomizing search	-Performance evaluation
Fukushima, et al. (1977)	- Initial condensing/evaporating pressures and enthalpy must be specified prior to execution	Steady	Constant	-No desuperheater - Three and two zones for the condenser and evaporator, respectively	- Capillary tube	-Gradient descent	-Design of heat pump
Domanski and Didion (1984)	-Evaporator inlet quality, saturation temperature and superheating degree must be specified prior to execution	Steady	Constant	-No desuperheater - Three and two zones for the condenser and evaporator, respectively	- Capillary tube	-Gradient descent -Global search algorithm	-Design of heat pump
Stefanuk et al. (1992)	- Evaporator inlet quality and saturation temperature as well as condensing temperature must be specified prior to execution -Fixed superheating degree	Steady	Constant	- Three and two zones for the condenser and evaporator, respectively	-Thermostatic expansion valve	-Dichotomizing search	-Performance evaluation
Koury et al. (2001)	- Initial condensing/evaporating pressures and superheating degree must be specified prior to execution	Steady and transient	Variable	- No desuperheater - Distributed condenser and evaporator models	- Thermostatic expansion valve	- Simultaneous solver method - Successive substitution	- Control of heat pump
Hui and Spitler (2002)	- Fixed superheating degree, no subcooling degree - Fixed heat transfer coefficients	Steady	Constant	- No desuperheater - Two zones for both condenser and evaporator	- Not modeled	- Simultaneous solver method - Multivariable optimization	- Performance evaluation based on manufacturer data
Zhao et al. (2003)	- Zero subcooling or superheating degrees - Initial thermodynamic states of the cycle's variables must be specified prior to execution	Steady	Constant	- No desuperheater - Two and one zones for the condenser and evaporator, respectively	- Thermostatic expansion valve	- Dichotomizing search	- Evaluation of the system
Rigola et al. (2005)	- Fixed compressor discharged pressure	Steady and transient	Constant	- No desuperheater - Distributed condenser	- Fixed opening expansion valve	- Successive substitution	- Evaluation of reciprocating compressors

				and evaporator models			
Winkler et al. (2008)	- Multi-component framework - Fixed subcooling degree - Initial thermodynamic states of the cycle's variables specified by running each component prior to execution - Fixed overall heat transfer coefficients	Steady	Constant	- No desuperheater - Parallel evaporators - Three and two zones for the condenser and evaporator, respectively	- No information	- Non-linear simultaneous equation solver	- Examination of simultaneous algorithms effectiveness and robustness
Belman et al. (2009)	- Fixed superheating degree - Initial thermodynamic states of the cycle's variables must be specified prior to execution	Steady	Variable	- No desuperheater - Three and two zones for the condenser and evaporator, respectively	- Thermostatic expansion valve	- Simultaneous solver method	- Parameter evaluation based on manufacturer data
Our novel model:	- Multi-component framework (no branching of refrigerant) - Flexible superheating and subcooling degree - Initial thermodynamic states of the cycle's variables derived transparently from inlet conditions	Steady	Variable	- Adaptable region models for the three heat exchangers (One, two or three zones, depending on the specific performance of the system)	- Controllable opening electronic expansion valve	- Multivariable error minimization method	- Evaluation at off-design conditions - Integration with ground and load simulation tools for calculation of realistic annual performance factors - Evaluation of control strategies

Table 2: Main input and output variables for each component

	Input	**Output**
Compressor	η_{fr}, V_{sw}, $freq$, $A_{0\ldots4}$, P_1, P_2, T_1	W_{el}, $\dot{m}_{compr,}$ H_2
Desuperheater	P_2, $T_{2,}$ T_{d2}', C_{pd}, $\dot{m}_d$, $\dot{m}$	Q_d, T_{d2}
Condenser	P_2, H_{2}', T_{c3}, C_{pc}, $\dot{m}_c$, $\dot{m}$	Q_c, T_{c2}'
Expansion Valve	η_{expv}, A_{max}, $B_{0\ldots2}$, ρ_{3l}, P_2, P_4	$\dot{m}_{expv}$
Evaporator	P_4, $H_{4,}$ T_{e1}, C_{pe}, $\dot{m}_e$, $\dot{m}$	P_1, Q_e, T_{e4}

Table 3: Refrigerant junction state for the modeled case for each heat exchanger, where the second and third letters denote the initial and final zones of the refrigerant in the heat exchanger (gas, mixed or liquid)

Heat exchanger	Case	inlet junction	outlet junction
Desuperheater	DGG	2 gas	2' gas
	DGM	2 gas	2' mix
Condenser	CGG	2' gas	3 gas
	CGM	2' gas	3 mix
	CGL	2' gas	3 liquid
	CMM	2' mix	3 mix
	CML	2' mix	3 liquid
Evaporator	EMG	4 mix	1 gas

Table 4: Experimental conditions

Component	**Control variable**	**Values**
Compressor	*freq*	45, 60, 75, 90 Hz
Expansion valve	*step*	80 to 480
Condenser output	T_{c2}'	35°C
flow rate	G_c	16 $Lmin^{-1}$
Evaporator output	T_{e1}	-5, 0, 5°C
flow rate	G_e	25 $Lmin^{-1}$
Desuperheater	T_{d2}'	5, 17, 30°C
	T_{d2}	65°C

Table 5: Simulated and experimental pressure and enthalpy values for selected experiments

Condition T_{d2}' T_{e1}-T_{c2}'-T_{d2}	**Junction**	***P* [Mpa]**		***H* [kJkg^{-1}]**		**Relative Error [%]**
		Exp.	**Sim.**	**Exp.**	**Sim.**	
17 5-35-65	1	0.64	0.63	434.18	427.44	2.81
	2	2.05	2.09	473.83	467.94	2.15
	2'	2.04	2.09	443.22	440.94	2.31
	3	2.06	2.09	281.80	281.74	1.26
	4	0.69	0.70	281.80	281.74	0.88
5 0-35-65	1	0.44	0.45	422.31	426.54	2.90
	2	2.07	2.07	476.94	479.34	0.51
	2'	2.02	2.07	435.85	435.94	2.57
	3	2.02	2.07	274.3	271.74	2.74
	4	0.57	0.56	274.3	271.74	2.37